Bulletin of the Seismological Society of America, Vol. 99, No. 2B, pp. 1251–1260, May 2009, doi: 10.1785/0120080090

Tilt Motions Recorded at Two WISE Sites for the 2003 Tokachi-Oki Earthquake (*M* 8.3)

by Shigeo Kinoshita, Hiroyuki Ishikawa, and Takashi Satoh

Abstract Broadband velocity seismographs installed at the Ohtsu water level observatory and Monsizu stations of the Warning Information System of Earthquake (WISE) network recorded long-period pulses produced by tilt motions resulting from the 2003 Tokachi-Oki earthquake (*M* 8.3) of 25 September 2003. The long-period pulse signal is represented using a low-pass-filtered expansion composed of intrinsic mode functions. By eliminating the leading phases, such as a direct *P* phase that appears before the onset of tilt motion from the expansion, the transient signal produced by the tilt motion is approximately obtained. A reverse filter, which is defined by the inverse of the frequency characteristics of the broadband velocity seismometer for the acceleration input, is applied to the transient signal to estimate the tilt motion. The estimated permanent acceleration of tilt motion at the two sites ranges from 0.6 to 6.5 cm/sec^2. The river embankment adjacent to the Ohtsu water level observatory site collapsed due to liquefaction at the bottom of the embankment. The Monsizu site was constructed at a depth of 2 m in soft soil floodplain deposits. These two broadband velocity seismograms involving the tilt motion reveal that the tilt motion is mainly generated under the influence of the collapsed soil structure or of the deformation of the soil deposits. These observations indicate that the broadband velocity seismograph is more sensitive to tilt motion than acceleration-type strong-motion seismographs.

Introduction

Large earthquakes cause the collapse of soil structures, such as soil embankments, and the destruction of soft soil deposits. Impacts to soil structures are induced by the rotational motion of the Earth's surface, as well as the translation motion. Recent strong-motion data suggest that tilt motion is generated in the region surrounding collapsed soil structures and in the soft soil deposits influenced by soil deformation (Holzer and Youd, 2007; Kinoshita, 2008). The present article reports observations derived from strong-motion records obtained using broadband velocity seismometers for the 2003 Tokachi-Oki earthquake (*M* 8.3) of 25 September 2003.

Recent increases in the availability of strong-motion data involving tilt motion in the near field are due to the development of broadband velocity seismometers, which are highly sensitive to tilt motion, in addition to existing acceleration-type seismographs. Broadband velocity seismometers measure frequencies with a high gain peak for tilt acceleration input and thus generate transient waves with long-period pulses. Broadband velocity seismometers produce remarkable long-period pulse signals, even for small tilt acceleration values in the range of 0.1–1 cm/sec^2, and the tilt motion is easily detectable in broadband velocity seismograms (Zahradník and Plešinger, 2005; Kinoshita, 2008).

Strong-motion observation using velocity seismometers in Japan has expanded with the development of the Muramatsu-type velocity seismometer (Muramatsu *et al.*, 2001). In the aftermath of the 1995 Kobe earthquake, VSE-type negative feedback velocity seismometers (Hutt *et al.*, 2008) have been used in many strong-motion observation networks, such as the F-net, a nationwide network in Japan, and the Warning Information System of Earthquake (WISE) net, comprised of 197 stations installed in Hokkaido with a station-to-station distance of approximately 40 km. In the present study, tilt motions recorded at two WISE stations for the 2003 Tokachi-Oki earthquake (*M* 8.3) using the VSE-355EI broadband velocity seismometer are investigated as typical examples of transient responses generated by tilt motions. One seismograph that recorded the tilt motion was installed at the Ohtsu water level observatory site, which is located in a soil embankment constructed along the Tokachi River. During the event, the embankment adjacent to the site collapsed due to liquefaction that occurred at the bottom of the embankment, although no collapse could be seen at the site. The other was installed in soft soil deposits at a depth of

2 m at the Monsizu site, which is located in the floodplain of the Oboro River. These recordings reveal that tilt motion is recorded even under the influence of slight soil deformation.

The output signal of the seismometer is a mixture of translations and rotations, and translational and rotational motions cannot be measured independently using inertial seismometers (Pillet and Virieux, 2007). However, a broadband velocity seismometer generates transient signals with long-period pulse by long-period tilt acceleration motion. Thus, the tilt motion in the acceleration domain can be estimated using the transient signal. In the present study, we propose a method for estimating the tilt acceleration by filtering the transient signal with long-period pulses. The details of the filtering are presented in the Method section. A difficult problem encountered in the approximate estimation of tilt motion using broadband velocity seismograms is determining a method by which to refine the identification of the transient signal generated by tilt motion. In the present article, a method using empirical mode decomposition (EMD) proposed by Huang *et al.* (1998) is applied to the identification of long-period pulse waves on broadband seismograms involving a transient signal. The details of the identification procedure are also presented in the Method section.

Data

The 2003 Tokachi-Oki earthquake (*M* 8.3) of 25 September 2003, occurred off the southern coast of Hokkaido at the boundary zone between the Pacific plate and the North American plate (Fig. 1). This event caused substantial damage in the Pacific coastal areas of Hokkaido. Strong-motion data, which are three-component broadband velocity seismograms, were recorded at 146 WISE stations (Ikeda *et al.*, 2003) for this event. The frequency characteristics of the broadband velocity seismometer VSE-355EI at each station are shown in Figure 2 (solid line). The dotted line is the velocity response for acceleration input. The characteristics of the peak indicate that the VSE-355EI seismometer is highly sensitive to long-period acceleration tilt signals with a frequency of approximately 0.02 Hz. The dot-dashed line denotes the frequency characteristics of the VSE-355EI broadband velocity seismometer for the input of the derivative of acceleration. A filter having the reverse characteristics is used to estimate tilt motion, as is described in the Method section. The maximum measurable velocity and the sampling rate of the data acquisition system used in the WISE network are 200 cm/sec and 100 Hz, respectively.

The broadband seismograms used in the present study were recorded at the Ohtsu water level observatory (I807K003; 42.6875° N, 143.6514° E) and Monsizu (I903K002; 43.0561° N, 144.7806° E) stations shown in Figure 1. The Ohtsu water level observatory site is located in a soil embankment constructed at the mouth of the Tokachi River, approximately 100 km from the epicenter. The Monsizu site is installed in soft soil deposits in the floodplain of the Oboro River, approximately 150 km from the epicenter. At both sites, a three-component broadband velocity seismometer was installed at a depth of 2 m, with the north–south (NS), east–west (EW), and up–down (UD) orientations.

Over 100 m of the embankment adjacent to the Ohtsu water level observatory site collapsed due to liquefaction at the bottom of the embankment, although indications of the collapse could not be detected at the site (Nishimoto, 2003). However, it is reasonable to consider that the Ohtsu water level observatory site was influenced by the soil deformation produced by the collapse of the embankment. The NS direc-

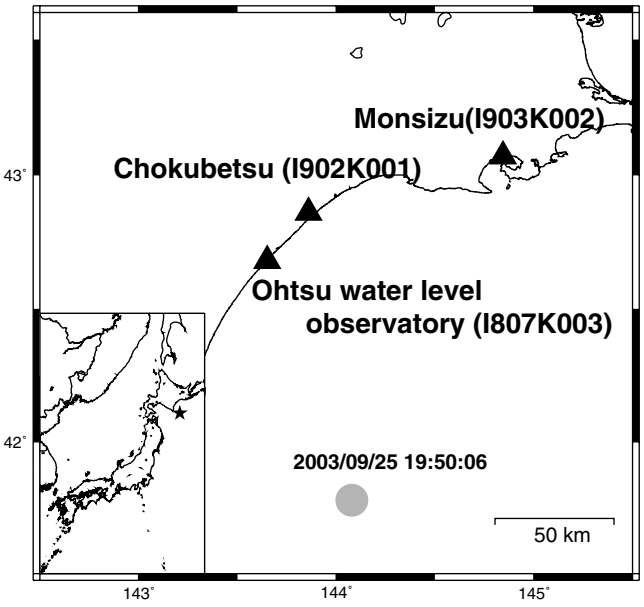

Figure 1. Epicenter of the 2003 Tokachi-Oki earthquake (*M* 8.3) (solid circle) and the locations of the Ohtsu water level observatory (I807K003), Monsizu (I903K002), and Chokubetsu (I902K001) sites.

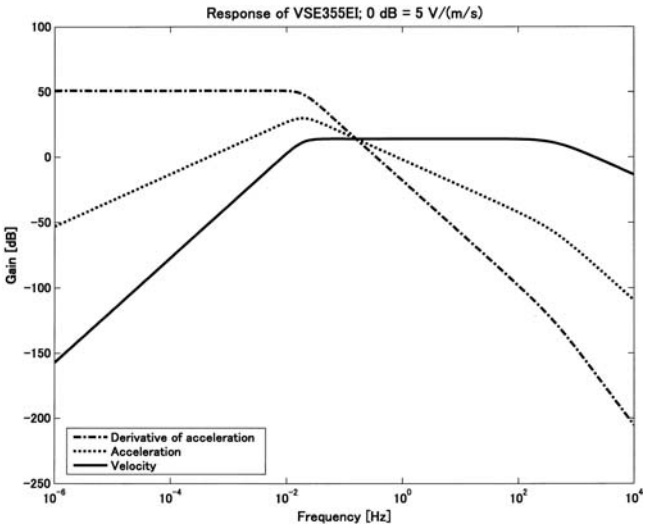

Figure 2. Frequency characteristics of a VSE-355EI broadband seismometer: solid, dotted, and dot-dashed lines represent the output characteristics for velocity, acceleration, and the derivative of acceleration inputs, respectively (0 dB = 5 V/m/sec).

tion of the Ohtsu water level observatory site is orthogonal to the river embankment, that is, the EW direction is along the embankment. The original three-component broadband velocity seismogram recorded at the Ohtsu water level observatory site shown in Figure 3 indicates that tilt motion occurred in the NS direction, toward which the collapsing embankment tilted. This means that the soil deformation in the embankment extended beneath the Ohtsu water level observatory site, although the collapse of the embankment did not extend to the site.

The original three-component broadband velocity seismogram recorded at the Monsizu site shown in Figure 4 indicates remarkable one-sided signals in the north and west directions. Although we have no information on damage near the site, it is reasonable to consider that the slight deformation of the soft floodplain deposits of the Oboro River is likely to have caused the tilt motion of the seismometer. The amount of one-sided horizontal movement at the Monsizu site is approximately 10% to 20% of that in the NS component at the Ohtsu water level observatory site.

At other WISE stations near the Ohtsu water level observatory and Monsizu sites, dominate long-period pulse waves on broadband seismograms were not recorded. This reveals that the tilt motions at these two sites are mainly due to local effects.

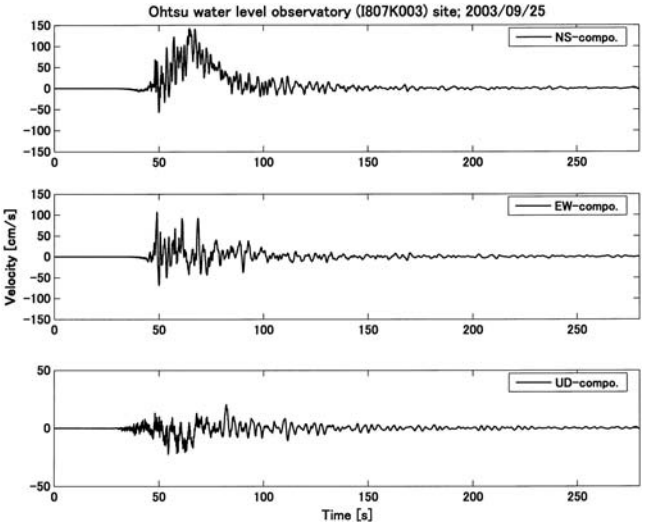

Figure 3. Three-component original velocity seismograms recorded at the Ohtsu water level observatory site for the 2003 Tokachi-Oki earthquake (*M* 8.3): NS (top panel), EW (center panel), and UD components (bottom panel).

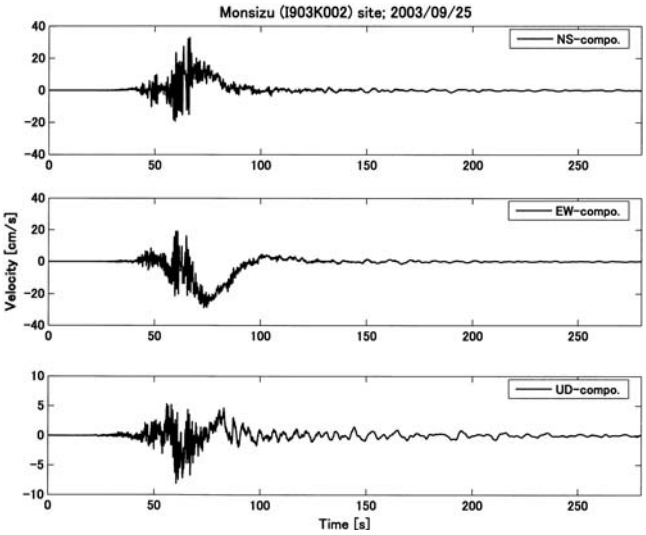

Figure 4. Three-component original velocity seismograms recorded at the Monsizu site for the 2003 Tokachi-Oki earthquake (*M* 8.3): NS (top panel), EW (center panel), and UD components (bottom panel).

Method

Methods for the approximate estimation of tilt motion using seismograms were previously proposed by Zahradník and Plešinger (2005), Graizer (2006), Pillet and Virieux (2007), and Kinoshita (2008). Among them, the method used in Kinoshita (2008) is directly applicable to broadband velocity seismograms. Each WISE station is equipped with a VSE-355EI, a three-component negative feedback broadband seismometer for strong-motion observation. Consequently, in the present study, tilt motion is estimated from long-period pulses on broadband velocity seismograms using an estimation model constructed in the Laplace domain, as demonstrated by Kinoshita (2008). The broadband velocity signal $V_0(s)$ in which the tilt motion $A(s)$ is superimposed linearly upon the translation motion $V(s)$ is given by

$$V_0(s) = V_v(s) + V_a(s) = G_0(s)V(s) + s^{-1}G_0(s)A(s), \tag{1}$$

where $V_v(s)$ is the broadband signal for the translation motion and $V_a(s)$ is the broadband signal for the tilt motion. The transfer function $G_0(s)$ is the response of the broadband velocity seismometer, which is given by the manufacture as follows:

$$G_0(s) = 39s/(0.002932s^3 + 7.808s^2 + 1.264s + 0.1112) \quad (\mathrm{V/m/sec}).$$

The amplitude character of $G_0(s)$ is shown by the solid line in Figure 2. In this figure, 0 dB = 5 V/m/sec. Hence, the tilt motion is estimated from

$$A(s) = [s^{-1}G_0(s)]^{-1}V_a(s) \tag{2}$$

by integrating $sA(s) = s^2G_0^{-1}(s)V_a(s)$. The inverse filter $s^2G_0^{-1}(s)$, defined as the inverse of the dot-dashed line in Figure 2, is shown by the dotted line in Figure 5. In this figure, the solid line is an approximate filter of

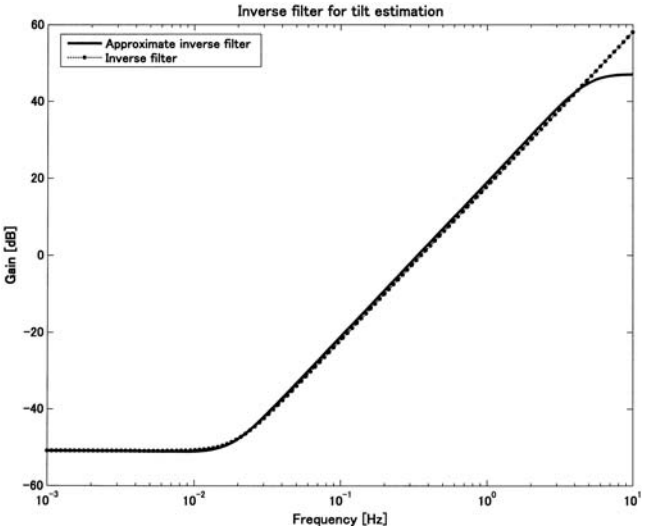

Figure 5. Frequency characteristics of the inverse filter used to estimate tilt motion in the derivative domain of acceleration (dotted line). The solid line indicates its approximate second-order filter (Kinoshita, 2008).

$s^2G_0^{-1}(s)$, replaced by a second-order system (Kinoshita, 2008) to suppress the high-frequency oscillation generated in $s^2G_0^{-1}(s)V_a(s)$.

In the previous method, the development of a method for identifying the transient signal $V_a(s)$ excited by tilt motion using long-period pulses on a broadband seismogram has yet to be resolved (Kinoshita, 2008). In the previous study, cascaded median filtering was used for this identification, which provided a robust estimation of permanent tilt acceleration. The cascaded median filter uses two rather long data windows. Accordingly, the smoothing of the transient signal using the cascaded median filtering is a delicate task for the calculation of the displacement seismogram using the velocity seismogram after eliminating the transient signal. To facilitate this task, we apply the EMD method and the associated Hilbert spectral analysis proposed by Huang *et al.* (1998) to the transient signal identification problem. The EMD breaks down the transient signal into its component intrinsic mode functions (IMFs). An IMF is a function that has only one extreme between zero crossings and has a mean value of zero. Huang *et al.* (1998) referred to the process to decompose the signal into IMFs as the shifting process. The shifting process is described briefly as follows:

1. From the original signal $v_0(t)$ $(0 \le t \le T)$, construct a new function: $r(t) = v_0(t)$.
2. Set $h(t) = r(t)$.
3. For the function $h(t)$, let $m_{10}(t)$ be the mean of its upper and lower envelopes, as determined from a cubic spline interpolation of the local maxima and minima of $h(t)$.
4. Set $h_{10}(t) = h(t) - m_{10}(t)$, that is, $h(t) = h_{10}(t) + m_{10}(t)$. This is the first shifting process.
5. In the second shifting process, replace $h(t)$ with $h_{10}(t)$ in (2) and repeat (3) and (4). The second shifting process yields the function $m_{11}(t)$, as determined by the mean of the upper and lower envelopes of $h_{10}(t)$. Using $m_{11}(t)$, construct a function $h_{11}(t) = h_{10}(t) - m_{11}(t)$, that is, $h_{10}(t) = h_{11}(t) + m_{11}(t)$.
6. Repeat this shifting procedure, that is, (5), k times, until the sum of the difference, SD is smaller than a preassigned value, ε, as follows:

$$SD = \sum_{t=0}^{T} \frac{|h_{1(k-1)}(t) - h_{1k}(t)|^2}{h_{1(k-1)}^2(t)} = \sum_{t=0}^{T} \frac{|m_{1k}(t)|^2}{h_{1(k-1)}^2(t)} < \varepsilon.$$

The value of $\varepsilon = 0.3$ is commonly used in literature (e.g., Huang *et al.*, 1998) and is used in the present study.
7. Set $x_1(t) = h_{1k}(t)$ as the first IMF, that is, a function that contains the shortest period component of the signal, $v_o(t)$.
8. Set $r_1(t) = r(t) - x_1(t)$ and then replace $r(t)$ with $r_1(t)$ in (2). Repeat the previous procedure from (3) to (7). The results are as follows:

$$r_2(t) = r_1(t) - x_2(t), \qquad r_3(t) = r_2(t) - x_3(t),$$
$$\ldots, \quad r_N(t) = r_{N-1}(t) - x_N(t).$$

The function $x_N(t)$ is the final IMF, which contains the longest period component of $v_0(t)$, that is, $2T$.
9. As a result, we get a set of IMFs, $\{x_k(t)\}_{k=1}^N$ and $v_0(t) = \sum_{k=1}^N x_k(t) + r_N(t)$, where $r_N(t)$ is the residue function, which can be a signal having one extreme, a monotonic mean trend, or a constant.

Thus, the number of a set of IMFs, N, depends on the signal, $v_0(t)$. Flandrin *et al.* (2004) and Wu and Huang (2004) showed that a set of IMFs is a set of band-pass-filtered waves. As described subsequently, this is a basic property of IMFs required for solving relation (1).

The EMD method was proven to be valid for application in the study of nonstationary strong-motion data (Huang *et al.*, 2001; Loh *et al.*, 2001). This method represents the time-domain signals $v_0(t)$ and $v_a(t)$, which correspond to $V_0(s)$ and $V_a(s)$, respectively, in the Laplace domain, as follows:

$$v_0(t) \approx \sum_{n=1}^{N} x_n(t), \qquad v_a(t) \approx \sum_{n=N_1+1}^{N} x_n(t), \qquad (3)$$

where $\{x_n(t)\}_{n=1}^N$ is a set of IMFs calculated from the original velocity data, $v_0(t)$. Namely, the long-period pulse wave involving the transient signal is obtained using an expansion, $\sum_{n=N_1+1}^N x_n(t)$. This means that the broadband velocity signal is separated into the translation signal, $\sum_{n=1}^{N_1} x_n(t)$, that is, a high-pass filtered expansion, and the tilt signal, $\sum_{n=N_1+1}^N x_n(t)$, that is, a low-pass-filtered expansion. These two pass bands of filtering do not overlap so that relation (1) is solved for $V_v(s)$ and $V_a(s)$ using two expansions of IMFs represented by relation (3). However, this separation in the

frequency domain is not based on physical grounds, although it is a basic technique commonly used for the estimation of tilt motion in the time domain by means of the filtering of seismic waves (Graizer, 2006; Kinoshita, 2008). Thus, the proposed method is an approximate method for the estimation of tilt motion, and its practical utility must be validated. In the Validation section, the practicality of the proposed method is verified using a synthesized wave.

In relation (3), the parameter N_1 must be determined in order to cover the power spectrum of the long-period pulse signal by that of the low-pass-filtered expansion in low frequencies, because the long-period pulse signal involves the transient signal generated by tilt motion. In practice, $N_1 + 1$ is determined by the maximum value on the condition that the low-pass-filtered expansion is in agreement with the long-period pulse signal. Although this determination of $N_1 + 1$ is visually possible, mathematically speaking, $N_1 + 1$ is determined by the maximum value on the condition that the Fourier amplitude spectrum of $\sum_{n=N_1+1}^{N} x_n(t)$ agrees with that of the long-period pulse signal at low frequencies. As a confirmation procedure for determining $N_1 + 1$, it may be practical to check that the estimated tilt motion obtained using $\sum_{n=N_1+1}^{N} x_n(t)$ agrees with that obtained using $\sum_{n=N_1}^{N} x_n(t)$ with the help of a post smoothing (low-pass) filter. The robustness of such a determination of N_1 will be discussed in the Validation section.

The EMD method is applicable to the solution for the identification problem of long-period pulse wave because the transient signal itself is similar to an IMF, as explained in the straightforward simulation described subsequently. Furthermore, the low-pass filtering based on the EMD method is free from the problems of group delay and settling time for the identification of long-period pulses in the time domain, which are problems inherent in standard filtering using a minimum-phase or linear-phase filter. Although median filtering may resolve these problems (Kinoshita, 2008), there is only one adjustable parameter, that is, window length. Thus, the EMD-based filter may be superior to the median filter for the time-domain identification of long-period pulses.

Let us now consider an example of the tilt acceleration motion, which is defined by a ramp function with a permanent acceleration of 5 cm/sec^2 and a 10 sec tilt increment, as shown by the thin solid curve in Figure 6, as input to the VSE-355EI broadband seismometer, resulting in the calculated transient wave shown by the thick solid curve in the same figure. This transient signal is decomposed into three IMFs, which are denoted C_1, C_2, and C_3 modes, as shown by the dotted curves in Figure 7. The primary mode is C_1, and the other two modes depend on the data length used for the IMF calculation. The transient signal is itself similar to the primary mode, which confirms the advantage of using the EMD method. According to the three IMFs, $x_n(t)$ $(n = 1, 2, 3)$, which correspond to C_n $(n = 1, 2, 3)$, the Hilbert spectrum of $x(t) = \sum_{n=1}^{3} x_n(t)$ is given as follows:

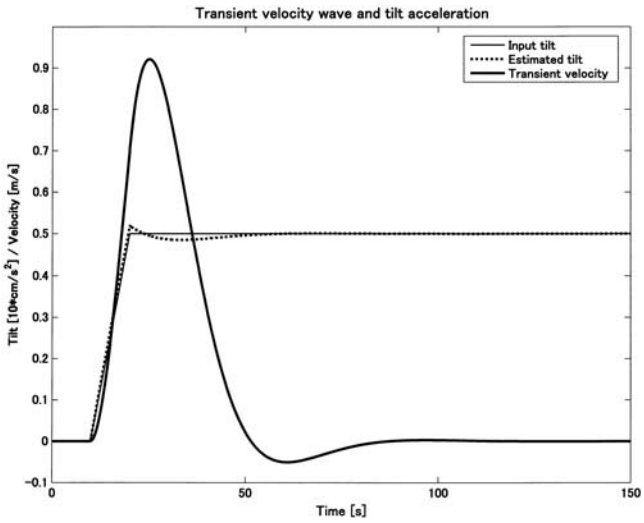

Figure 6. Simulated transient velocity wave (thick curve) of the VSE-355EI broadband seismometer for a tilt acceleration input with a ramp function type (thin curve). The dotted curve shows the estimated tilt motion derived from the transient wave shown by the solid curve.

$$
\begin{aligned}
z_n(t) &= x_n(t) + i\hat{x}_n(t) = a_n(t)e^{i\theta_n(t)},\\
a_n(t) &= [x_n^2(t) + \hat{x}_n^2(t)]^{1/2},\\
\theta_n(t) &= \arctan\left[\frac{\hat{x}_n(t)}{x_n(t)}\right] \qquad (n = 1, 2, 3),
\end{aligned} \tag{4}
$$

where $\hat{x}_n(t)$ is the Hilbert transform of $x_n(t)$. In practical application, the instantaneous frequency,

$$
\omega_n = \frac{d\theta_n(t)}{dt} \equiv 2\pi f_n(t), \tag{5}
$$

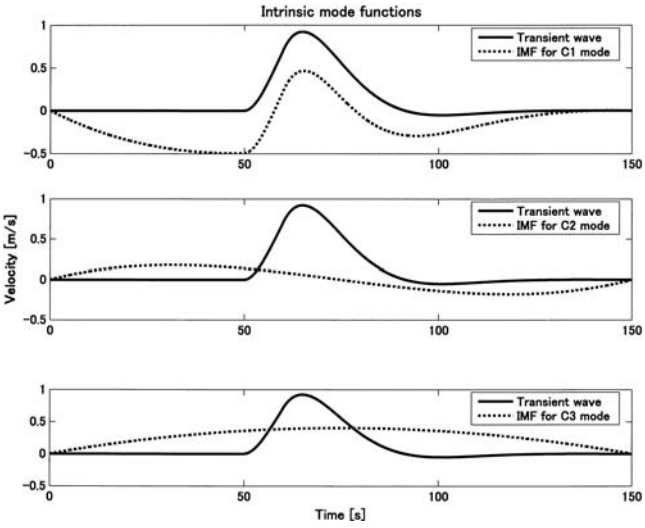

Figure 7. Transient velocity signal generated by tilt motion (solid curve) and IMFs of the signal (dotted curve): C_1 (top panel), C_2 (center panel), and C_3 (bottom panel) modes.

is used in the Hilbert spectral analysis instead of the phase function $\theta_n(t)$. Similarly, the instantaneous frequency f of the IMF expansion $x(t)$ is derived from relations (4) and (5) by replacing $x_n(t)$ with $x(t)$. The instantaneous frequencies of the three IMFs and $x(t)$ are shown in Figure 8. Although the instantaneous frequency can take negative values (Cohen, 1995), its nonnegative part is shown in this figure. With the exception of values at the edges of the data window, $f_2(t) \approx 1/150$ Hz and $f_3(t) \approx 1/300$ Hz. Namely, these two frequencies depend only on the window length. The instantaneous frequencies of $f_1(t)$ (thin curve) and $f(t)$ (dotted curve) trace the same movement as the transient signal shown by the thick curve in Figure 8. This figure reveals that the sudden increase point of $f(t)$ synchronizes with the onset of the transient signal, indicating that the instantaneous frequency trace for the IMF expansion $x(t)$ of the transient signal is likely to detect the onset of tilt phase. Thus, the onset time is determined by the sudden increase point or a local minimum point in the instantaneous frequency. In the Validation section, such synchronization between the transient signal and the instantaneous frequency will be discussed in detail for a seismic wave involving a transient pulse artificially generated by the tilt motion of a ramp function.

Validation

To validate the stability of proposed method for estimating tilt motion, the proposed method is applied to a synthesized wave composed of a real broadband velocity seismogram with no long-period pulses and a transient signal artificially generated by a tilt motion. The broadband signal is the NS component recorded at the Chokubetsu (I902K001; 42.8414° N, 143.8781° E) site for the 2003 Tokachi-oki earthquake (M 8.3) using a VSE-355EI seismometer, which is shown in the top panel of Figure 9. As shown in Figure 1, the Chokubetsu (I903K002) site is located between the Ohtsu water level observatory (I807K003) and the Monsizu (I903K002) sites. The transient signal shown in the bottom center panel of Figure 9 is artificially generated from the response of the VSE-355EI seismometer with an acceleration input shown in the top center panel of Figure 9. The input acceleration, that is a tilt motion, is a ramp function with a permanent acceleration of -10 cm/sec^2 and a dynamic duration of 10 sec. The synthesized wave is shown in the bottom panel of Figure 9.

A set of IMFs $\{x_n(t)\}_{n=1}^{N}$ is calculated using the synthesized wave. The number N of a set of IMFs is 14 for this synthesized wave. Thus, the long-period pulse wave is expanded by $\sum_{n=N_1+1}^{14} x_n(t)$. In Figure 10, the low-pass-filtered expansion, $\sum_{n=N_1+1}^{14} x_n(t)$, is shown for $N_1 + 1 = 7$, 8, 9, and 10 using the black curve along with the synthesized wave shown by the gray curve. The caption $C_{N_1+1} - C_{14}$ for each panel indicates that the results are obtained from the IMF expansion, $\sum_{n=N_1+1}^{14} x_n(t)$. The low-pass-filtered expansion for $N_1 + 1 = 10$ cannot trace the long-period pulse signal of the synthesized wave, as shown at the bottom right-hand panel of Figure 10. Similarly, for $N_1 + 1 > 10$, the low-pass-filtered expansion disagrees with the transient signal of the synthesized wave. Thus, $N_1 + 1 = 9$ is the maximum number for which the expansion, $\sum_{n=N_1+1}^{14} x_n(t)$ traces the transient signal. The dotted curves in Figure 10 show the instantaneous frequency of $\sum_{n=N_1+1}^{14} x_n(t)$ for $N_1 = 7$, 8, 9, and 10. The point indicated by the arrow is

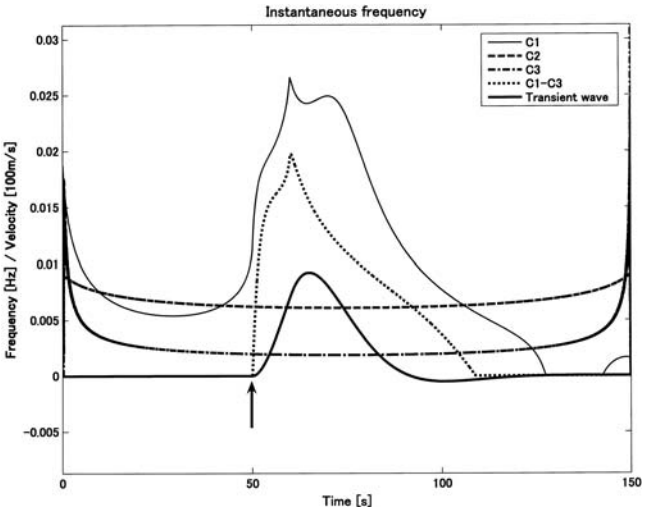

Figure 8. Instantaneous frequencies for intrinsic modes: C_1 (thin solid curve), C_2 (dashed curve), and C_3 (dot-dashed curve) modes. The dotted curve shows the instantaneous frequency of a function obtained by summing all IMFs. The thick solid curve is the transient signal used for the calculation of IMFs. The point indicated by the arrow is the sudden increase point in the instantaneous frequency shown by the dotted curve.

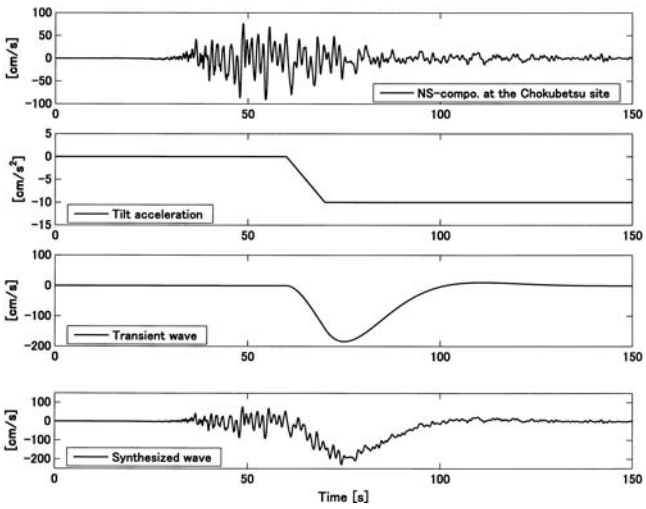

Figure 9. Synthesized wave (bottom panel) used for the validation of the proposed tilt estimation method. The synthesized wave is comprised of the NS-component seismogram (top panel) recorded by the VSE-355EI broadband seismometer installed at the Chokubetsu site and the transient signal (bottom center panel) artificially generated by a tilt acceleration with a ramp function type (top center panel).

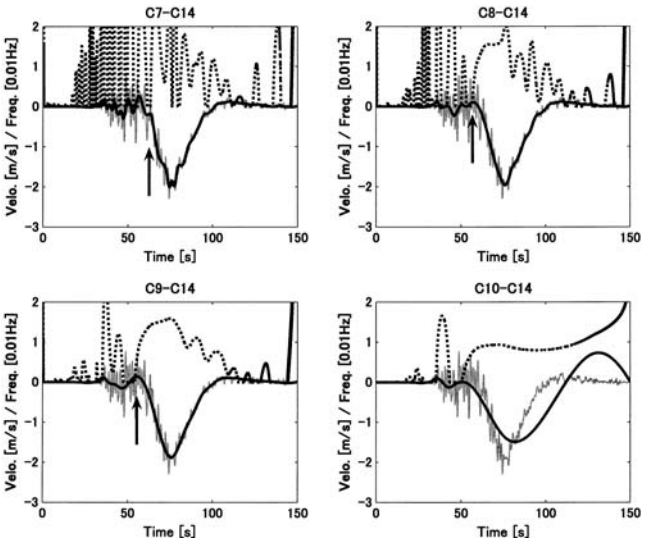

Figure 10. Low-pass-filtered wave (black curve) and its instantaneous frequency (dotted curve) calculated from the synthesized seismogram (gray curve) shown in the bottom panel of Figure 9. The low-pass-filtered wave, $\sum_{k=N_1+1}^{14} x_k(t)$, is comprised by summing the IMFs from $N_1 + 1 = 7$ (top left-hand panel), 8 (top right-hand panel), 9 (bottom left-hand panel), and 10 (bottom right-hand panel) to $N = 14$.

the onset of tilt motion determined for each low-pass-filtered expansion.

Applying the proposed method to these low-pass-filtered expansions for $N_1 + 1 = 7$, 8, and 9, tilt motions are estimated as shown in Figure 11. The top, center, and bottom panels of Figure 11 are tilt motions estimated for the low-pass-filtered expansions, $\sum_{n=N_1+1}^{14} x_n(t)$ for $N_1 + 1 = 7$, 8, and 9, respectively. The thick curve is the smoothed tilt motion of the raw tilt motion shown by the dotted curve. The smoothing is performed using a median filter. The results in Figure 11 indicate that for $N_1 + 1 = 7$, 8, and 9 the smoothed tilt motion is in good agreement with the original tilt motion shown by the thin curve, which is used for the generation of the transient signal. Hence, the results shown in Figure 11 indicate that in the proposed estimation procedure of tilt motion using IMF expansion, the choice of N_1 is robust and the smoothed tilt motion is stable.

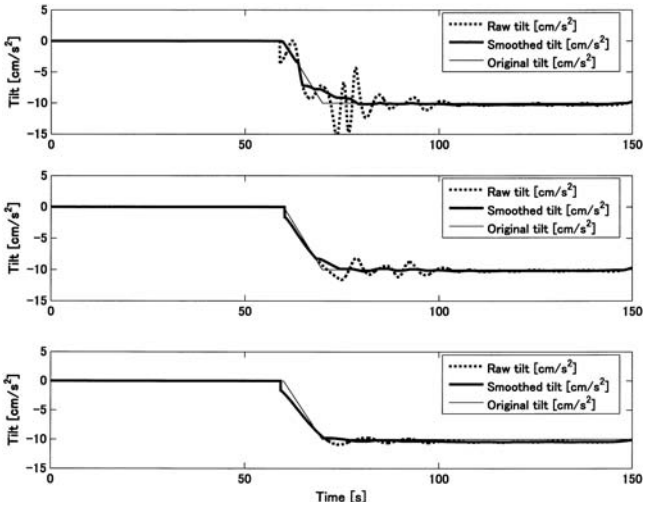

Figure 11. Tilt signals estimated using the low-pass-filtered wave, $\sum_{k=N_1+1}^{14} x_k(t)$, comprised by summing the IMFs from $N_1 + 1 = 7$ (top panel), 8 (center panel), and 9 (bottom panel) to $N = 14$, which is a raw estimate of the tilt signal (dotted curve) and its smoothed tilt signal (thick curve). The original tilt signal is shown by the thin curve.

This robustness of the choice of N_1 is partially due to the smoothing process of the raw estimate of tilt motion. In panels of Figure 12, the Fourier amplitude spectrum of the low-pass-filtered expansion, $\sum_{n=N_1+1}^{14} x_n(t)$ for $N_1 + 1 = 7$, 8, 9, and 10, is shown by the solid curve. The caption $C_{N_1+1} - C_{14}$ for each panel indicates that the results are obtained from the IMF expansion, $\sum_{n=N_1+1}^{14} x_n(t)$. For the calculation of the Fourier spectrum, the data of $60 \le t \le 150$ sec shown by the solid curve in Figure 10 is used because the onset of tilt motion is $t = 60$ sec. The dotted curve is the Fourier amplitude spectrum of the transient signal shown at the bottom center panel of Figure 9. Thus, the low-pass-filtered expansion, $\sum_{n=N_1+1}^{14} x_n(t)$, is the best estimate of the transient signal when the Fourier amplitude spectrum of $\sum_{n=N_1+1}^{14} x_n(t)$ agrees with the Fourier amplitude spectrum shown by the dotted curve. These Fourier amplitude spectra are quite different for $N_1 + 1 = 10$, as shown at the bottom right of Figure 12. The difference becomes greater for $N_1 + 1 > 10$. For $N_1 + 1 = 7$, 8, and 9, the Fou-

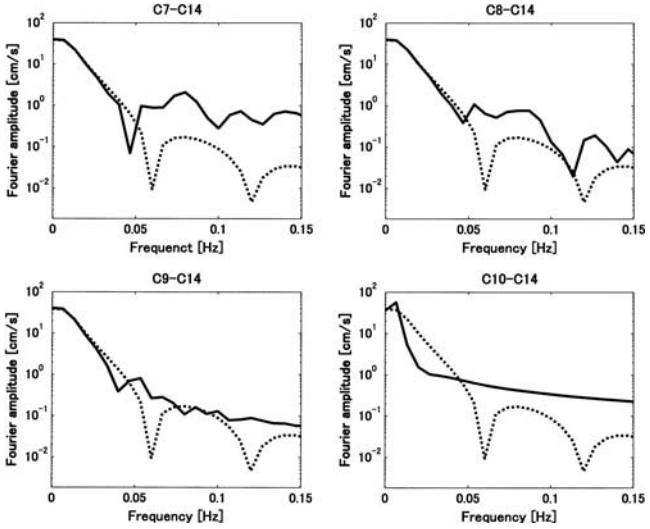

Figure 12. Fourier amplitude spectrum of the transient signal shown in the bottom center panel of Figure 9 (dotted curve) and that of the low-pass-filtered wave, $\sum_{k=N_1+1}^{14} x_k(t)$ (solid curve), comprised by summing the IMFs from $N_1 + 1 = 7$ (top left-hand panel), 8 (top right-hand panel), 9 (bottom left-hand panel), and 10 (bottom right-hand panel) to $N = 14$. The Fourier amplitude spectra are calculated using data in a time window of from 60 to 150 sec in the time scale in Figures 9 and 10. The notch structure in the Fourier amplitude spectrum of the original tilt signal is smoothed over in the Fourier amplitude spectrum of the low-pass-filtered wave. This is due to the lack of high-frequency components in the filtered wave.

rier amplitude spectrum of the low-pass-filtered expansion, $\sum_{n=N_1+1}^{14} x_n(t)$, is in good agreement with that of the transient signal at frequencies below approximately 0.036 Hz, that is, double of the resonance frequency in the response of the VSE-355EI seismometer for an acceleration input, the frequency at which the peak response is produced, as shown by the dotted line in Figure 2. However, for $N_1 + 1 = 7$, the Fourier amplitude spectrum of the low-pass-filtered expansion at frequencies above 0.05 Hz is much larger than that of the transient signal, as shown in the top left-hand panel of Figure 12. Thus, a smoothing filter, that is, a type of low-pass filter, is required for the estimation of tilt motion, as shown in the top panel of Figure 11. This overvalue in the Fourier amplitude spectrum increases with the decrease of $N_1 + 1$. For $N_1 + 1 = 9$, the Fourier amplitude spectrum of the low-pass-filtered expansion, $\sum_{n=9}^{14} x_n(t)$, agrees well with that of the transient signal, as shown in the bottom left-hand panel of Figure 12, so that the smoothing filter is insignificant, as shown at the bottom panel of Figure 11. For $N_1 + 1 = 8$, the matching of two Fourier spectra at frequencies below 0.05 Hz is superior, as compared with the Fourier matching for $N_1 + 1 = 9$, as shown in the top right-hand panel of Figure 12. This Fourier matching yields a good agreement between the estimation of permanent tilt, as shown in the center panel of Figure 11. These results reveal that the low-pass-filtered expansion, $\sum_{n=N_1+1}^{14} x_n(t)$, with the largest number of $N_1 + 1$ for which the low-pass-filtered expansion traces the long-period pulse wave on a broadband seismogram is used for the estimation of tilt motion. However, the expansion, $\sum_{n=N_1}^{N} x_n(t)$ can also possibly be used for the estimation of tilt motion with the help of a post smoothing filter. Among these two expansions, the best selection is probably data dependent.

In the simulation study described previously, the onset of tilt motion is fixed at a lapse time of 60 sec in the time scale used in Figure 9. For other different onsets of tilt motion, the proposed method yields similar estimates of tilt motions. This also indicates the stability of the proposed method.

Results

Seventeen IMFs, $\{x_n(t)\}_{n=1}^{17}$, are obtained using the shifting process from the NS-component data with a duration of 280 sec recorded at the Ohtsu water level observatory site. The total number of IMFs, $N = 17$ depends on the data. The expansion $\sum_{k=N_1+1}^{N=17} x_k(t)$ for $N_1 + 1 = 9$, 10, 11, and 12, shown by the black curves in the panels of Figure 13, represents the low-pass-filtered components of the original velocity seismogram shown by the gray curves. The caption $C_{N_1+1} - C_{17}$ for each panel indicates that the results are obtained from the IMF expansion, $\sum_{n=N_1+1}^{17} x_n(t)$. Visually, $N_1 + 1 = 11$ may be the largest number by which the expansion $\sum_{k=N_1+1}^{N=17} x_k(t)$ traces the long-period pulse wave on the broadband seismogram; and thus the results shown in the panel with the caption $C_{11} - C_{17}$ are used for the identification of long-period pulse wave. In the panels of Figure 13, the dotted curves represent the instantaneous frequency of $\sum_{k=N_1+1}^{N=17} x_k(t)$ for $N_1 + 1 = 9$, 10, 11, and 12. The onset of the transient phase is possibly the point that is allowed, that is, the point at which the instantaneous frequency is locally minimum for $N_1 + 1 = 10$ and 11. The solid curve in Figure 14 is the estimated transient wave for $N_1 + 1 = 11$. The leading time series of the expansion $\sum_{k=N_1+1}^{N=17} x_k(t)$ must be zero until the onset of the tilt phase. Applying the estima-

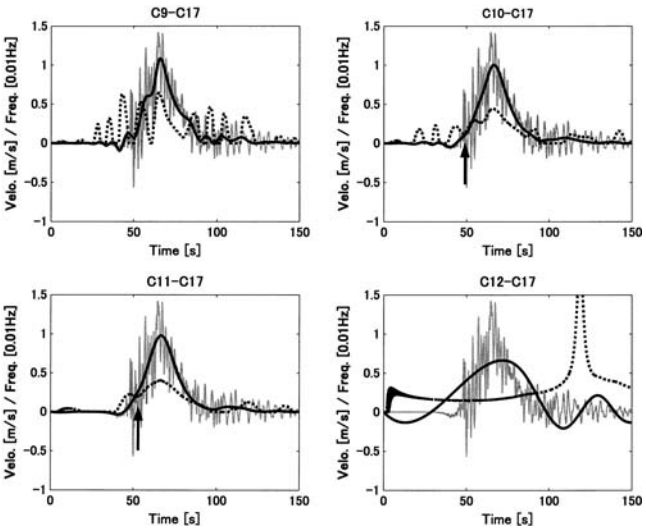

Figure 13. Low-pass-filtered wave (black curve) and its instantaneous frequency (dotted curve) calculated from the NS-component seismogram (gray curve) recorded at the Ohtsu water level observatory site. The low-pass-filtered wave, $\sum_{k=N_1+1}^{17} x_k(t)$, is comprised by summing the IMFs from $N_1 + 1 = 9$ (top left-hand panel), 10 (top right-hand panel), 11 (bottom left-hand panel), and 12 (bottom right-hand panel) to $N = 17$.

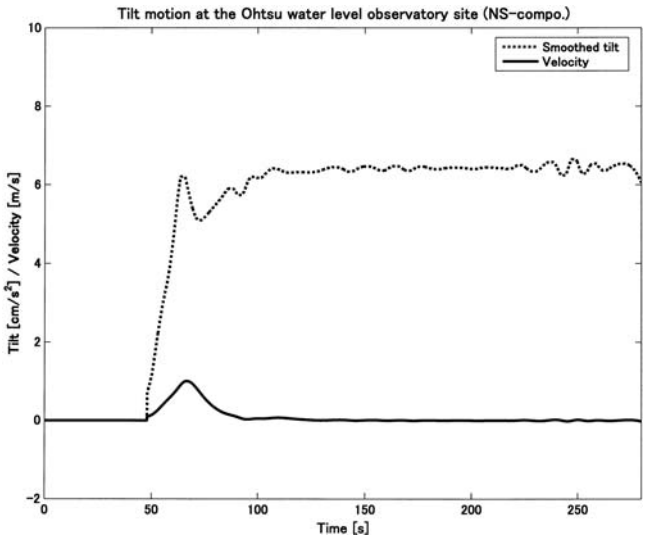

Figure 14. Estimated tilt motion in the acceleration domain (dotted curve) for the NS component at the Ohtsu water level observatory site and estimated transient signal (solid curve) used for estimation of the tilt signal.

tion procedure explained in the Method section to this transient wave, the tilt acceleration is obtained as shown by the dotted curve in Figure 14, which is smoothed by a median filter. The results indicate a tilt motion with a permanent acceleration of approximately 6.5 cm/sec^2. This means that the seismometer tilted in the south direction, which is the direction toward the bottom of embankment. The duration of dynamic tilting is approximately 10 sec.

The total number of IMFs is determined as $N = 17$ and $N = 14$ for the NS and EW components, respectively, at the Monsizu site. The expansion $\sum_{k=N_1+1}^{N=17} x_k(t)$ for $N_1 + 1 = 9$, 10, 11, and 12, shown by the black curves in the panels of Figure 15, represents the low-pass-filtered components for the NS component of the original seismogram shown by gray curves. Similarly, for the EW component, four low-pass-filtered expansions are shown in Figure 16. The largest number of $N_1 + 1$ may be 10 for both NS and EW components, which is visually determined without the help of a Fourier amplitude spectrum. Thus, long-period pulse waves in the broadband velocity seismograms recorded at the Monsizu site may be represented by expansions $\sum_{k=10}^{17} x_k(t)$ and $\sum_{k=10}^{14} x_k(t)$ for the NS and EW components, respectively. The allowed points on the instantaneous frequencies in the panels of Figures 15 and 16 are the most probable onsets of tilt phase for the NS and EW components, respectively. The identified long-period pulse waves involving the transient waves produced by tilt motion are shown by solid curves in the top and bottom panels of Figure 17 for the NS and EW components, respectively. Similarly, the estimated tilt accelerations are shown by the dotted curves in the top and bottom panels of Figure 17 for the NS and EW components,

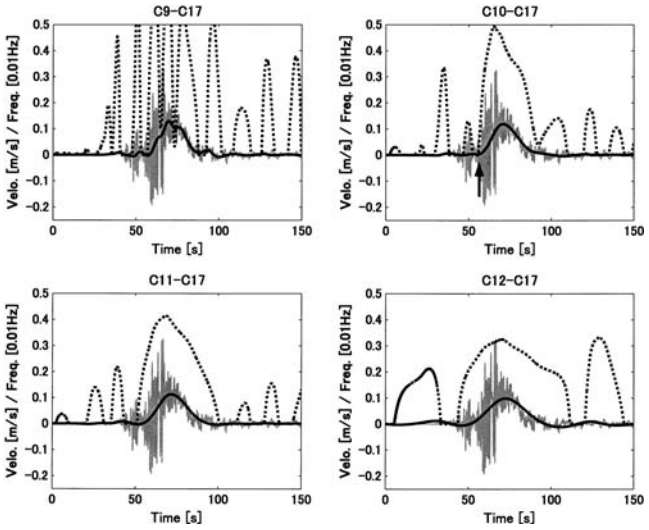

Figure 15. Low-pass-filtered wave (black curve) and its instantaneous frequency (dotted curve) calculated from the NS-component seismogram (gray curve) at the Monsizu site. The low-pass-filtered wave, $\sum_{k=N_1+1}^{17} x_k(t)$, is comprised by summing the IMFs from $N_1 + 1 = 9$ (top left-hand panel), 10 (top right-hand panel), 11 (bottom left-hand panel), and 12 (bottom right-hand panel) to $N = 17$.

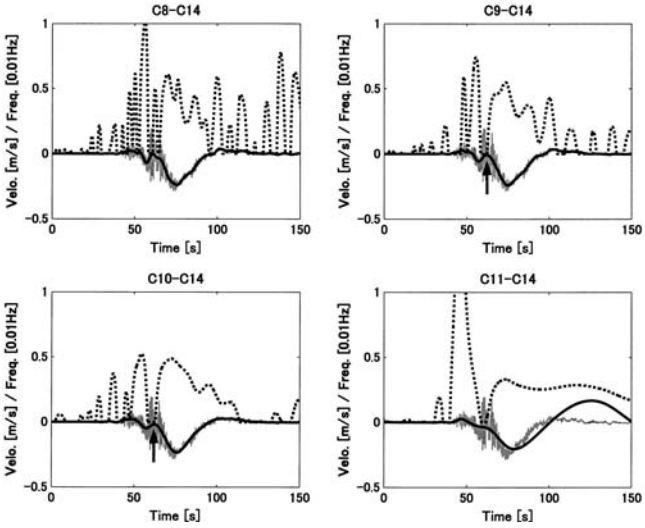

Figure 16. Low-pass-filtered wave (black curve) and its instantaneous frequency (dotted curve) calculated from the EW-component seismogram (gray curve) at the Monsizu site. The low-pass-filtered wave, $\sum_{k=N_1+1}^{14} x_k(t)$, is comprised by summing the IMFs from $N_1 + 1 = 8$ (top left-hand panel), 9 (top right-hand panel), 10 (bottom left-hand panel), and 11 (bottom right-hand panel) to $N = 14$.

respectively. The permanent accelerations are approximately 0.6 cm/sec^2 and -1 cm/sec^2 for the NS and EW components, respectively. In particular, a permanent acceleration of 0.6 cm/sec^2 may be difficult to detect using an acceleration-type strong-motion seismograph.

Conclusions

The broadband velocity seismograms recorded at the Ohtsu water level observatory and Monsizu stations of the

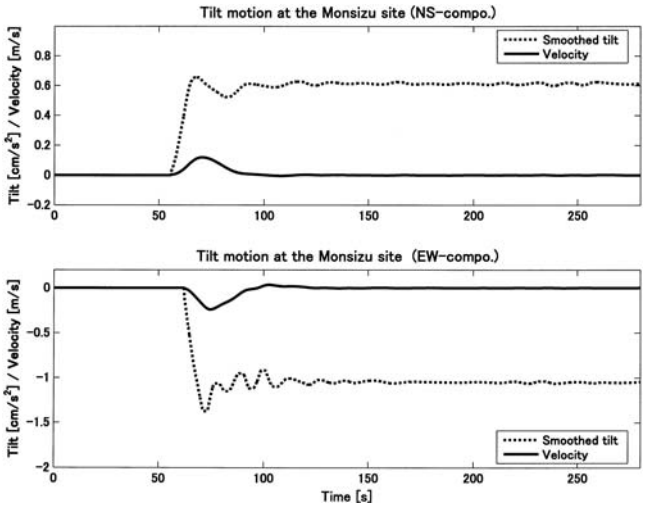

Figure 17. Estimated tilt signal in the acceleration domain (dotted curve) for the NS (top panel) and EW (bottom panel) components at the Monsizu site. The estimated transient signal shown by solid curve is used for estimation of the tilt signal.

WISE strong-motion network for the 2003 Tokachi-Oki earthquake (*M* 8.3) of 25 September 2003 involved remarkable long-period pulse waves generated by the tilt motion of a borehole seismometer installed at a depth of 2 m. The estimation of tilt motion using these broadband data yielded the following results:

1. The tilt motions recorded at the Ohtsu water level observatory and Monsizu sites were generated under the influence of the collapse of the soil embankment and under the influence of the deformation of soft soil deposits, respectively. The permanent accelerations of estimated tilt are 6.5 and 0.6–1 cm/sec^2 at the Ohtsu water level observatory and Monsizu sites, respectively. This reveals that the broadband velocity seismometer is highly sensitive to tilt motion and is able to detect permanent accelerations as low as 0.6 cm/sec^2.
2. To estimate tilt motion using long-period pulse signals on the broadband velocity seismograms, identification of the transient signal generated by tilt motion is required. The expansion comprised of IMFs calculated from the long-period pulse signal involves the transient signal. The tracing of the instantaneous frequency of the low-pass-filtered expansion of IMFs provides information indicating the onset of tilt phase. This means that the transient signals could be identified using the EMD method. The advantage of using EMD is based on the fact that the transient signal itself is similar to an IMF.

Data and Resources

Seismograms used in the present study were collected by the Civil Engineering Research Institute for Cold Region, Japan, and are not released to the public.

Acknowledgments

We are grateful to the anonymous reviewers for their comments and suggestions, which helped to improve the manuscript.

References

Cohen, L. (1995). *Time-Frequency Analysis*, Prentice Hall, Englewood Cliffs, New Jersey.

Flandrin, P., G. Rilling, and P. Goncalves (2004). Empirical mode decomposition as a filter-bank, *IEEE Signal Proc. Lett.* **11,** no. 2, 112–114.

Graizer, V. (2006). Tilts in strong ground motion, *Bull. Seismol. Soc. Am.* **96,** 2090–2102.

Holzer, T. L., and T. L. Youd (2007). Liquefaction, ground oscillation, and soil deformation at the Wildlife array, California, *Bull. Seismol. Soc. Am.* **97,** 961–976.

Huang, N. E., C. C. Chern, K. Huang, L. W. Salvino, S. R. Long, and K. L. Fan (2001). A new spectral representation of earthquake data: Hilbert spectral analysis of station TCU129, Chi-Chi, Taiwan, 21 September 1999, *Bull. Seismol. Soc. Am.* **91,** 1310–1338.

Huang, N. E., Z. Shen, S. R. Long, M. C. Wu, H. H. Shin, Q. Zheng, N. Yen, C. C. Tung, and H. H. Liu (1998). The empirical mode decomposition and Hilbert spectrum for nonlinear and non-stationary time series analysis, *Proc. R. Soc. Lond. A* **454,** 903–995.

Hutt, C. R., J. R. Evans, and I. Yokoi (2008). A brief test of the Tokyo Sokushin VSE-355G3 strong motion velocity seismometer, *U.S. Geol. Surv. Open-File Rept. 2008-1311*, 1–44.

Ikeda, K., T. Sato, and S. Okada (2003). 2003 Tokachi-Oki earthquake and strong motion, Special issue on the 2003 Tokachi-Oki earthquake (*M* 8.0), *Mon. Rep. Civ. Eng. Res. Inst. Hokkaido*, 2–6 (in Japanese).

Kinoshita, S. (2008). Tilt measurement using broadband velocity seismograms, *Bull. Seismol. Soc. Am.* **98,** 1887–1897.

Loh, C. H., T. C. Wu, and N. E. Huang (2001). Application of the empirical mode decomposition—Hilbert spectrum method to identify near-fault ground-motion characteristics and structural responses, *Bull. Seismol. Soc. Am.* **91,** 1339–1357.

Muramatsu, I., T. Sasatani, and I. Yokoi (2001). Velocity-type strong-motion seismometer using a coupled pendulum: design and performance, *Bull. Seismol. Soc. Am.* **91,** 604–616.

Nishimoto, S. (2003). Damage of river embankments, Special issue on the 2003 Tokachi-Oki earthquake (*M* 8.0), *Mon. Rep. Civ. Eng. Res. Inst. Hokkaido*, 7–14 (in Japanese).

Pillet, R., and J. Virieux (2007). The effects of seismic rotations on inertial sensors, *Geophys. J. Int.* **171,** no. 3, 1314–1323, doi 10.1111/j.1365-246X.2007.03617.x.

Wu, Z., and N. Huang (2004). A study of the characteristics of white noise using the empirical mode decomposition method, *Proc. R. Soc. Lond. A* **460,** 1597–1611.

Zahradník, J., and A. Plešinger (2005). Long-period pulses in broadband records of near earthquakes, *Bull. Seismol. Soc. Am.* **95,** 1926–1939.

Yokohama City University
Seto 22-2, Kanazawa-ku
Yokohama 236-0027, Japan
(S.K.)

Civil Engineering Research Institute for Cold Region
Hiragishi 1-3-1-34, Toyohira-ku
Sapporo 062-8602, Japan
(H.I., T.S.)

Manuscript received 30 May 2008